RSC Applied Interfaces

ROYAL SOCIETY OF CHEMISTRY

COMMUNICATION

View Article Online
View Journal | View Issue

Check for updates

Cite this: *RSC Appl. Interfaces*, 2026, 3, 322

Received 13th August 2025,
Accepted 24th November 2025

DOI: 10.1039/d5lf00236b

rsc.li/RSCApplInter

Enhanced cycling stability of Ni-rich Li-metal cells enabled by dual vinylene carbonate and tris(trimethylsilyl)borate electrolyte additives

Zishuo Zhao,[a] Yunyuan Lu,[a] Yuwei Zhu,[a] Dennis Nordlund,[b] Sooyeon Hwang *[c] and Linqin Mu *[a]

NMC811 ($LiNi_{0.8}Co_{0.1}Mn_{0.1}O_2$) and other high-Ni chemistries are promising cathode candidates for high-performance electric vehicles, owing to their high energy density and reduced cobalt content. However, their long-term cycling stability is hindered by surface degradation, particularly when paired with conventional electrolytes and a lithium metal anode. Electrolyte additives represent a practical approach to enhance interfacial stability and improve overall battery performance by promoting the formation of a robust electrolyte–electrode interphase (EEI). In this study, we revisit the effects of vinylene carbonate (VC) and tris(trimethylsilyl)borate (TMSB) additives on single-crystal SC-NMC811||Li cells. While TMSB only increases the open-circuit voltage and initial overpotential, it delivers superior capacity retention at C/3 compared to cells containing only VC or a dual additive system (VC and TMSB). Notably, under fast-charging conditions (1C, 2C, and 5C), the dual-additive system significantly outperforms other formulations, achieving markedly enhanced long-term capacity retention. Comprehensive electrochemical and spectroscopic analyses reveal that the VC/TMSB dual-additive system suppresses surface transition in NMC811, mitigates structural degradation by forming a thin, LiF-deficient cathode-electrolyte interface (CEI) layer. Moreover, they promote smooth and dense Li deposition and generate a LiF-deficient solid-electrolyte interphase (SEI). Consequently, the synergistic stabilization of both the CEI and SEI effectively limits the overall cell impedance growth during extended cycling. These findings provide key insights into co-additive strategies for engineering stable interfaces in high-energy Ni-rich Li-metal batteries.

Introduction

Lithium-ion batteries (LIBs) have dominated and will continue to dominate the electric vehicle and energy storage markets due to their superior performance, offering high energy density, power density, and efficiency. Current LIB technology primarily uses cathode materials such as $LiFePO_4$ or layered oxides ($LiNi_xMn_yCo_{1-x-y}O_2$) paired with a graphite anode. However, the growing demand for higher energy density has increased interest in lithium metal anodes coupled with Ni-rich ($LiNi_xMn_yCo_{1-x-y}O_2$, $x \geq 0.6$) cathodes.[1] Thus, such a cell configuration (Ni-rich||Li) is considered the next step toward commercialization, as it maximizes the energy density of LIBs. However, their operation typically requires higher cutoff voltages (≥4.4 V), which accelerates side reactions and contributes to both bulk and surface degradation of electrode materials. For instance, Ni-rich cathodes usually undergo surface reconstruction, where the layered structure transforms into electrochemically inactive rock-salt or spinel phases due to oxygen loss and transition metal migration.[2,3] In addition, electrolyte oxidation at high voltages leads to an unstable cathode–electrolyte interphase (CEI), thus promoting more side reactions and TM dissolution.[4] These coupled surface and bulk degradation processes collectively compromise the structural integrity and electrochemical reversibility of NMC cathodes.

Several strategies have been explored to mitigate the surface degradation and improve stability and compatibility of layered cathode materials, including doping, coating, and electrolyte engineering.[5] For example, our previous results demonstrate that dual Mg/Ti-doping leads to surface-enrichment of Ti at the $LiNiO_2$ particle surface, which effectively enhances the surface oxygen and contributes to a more robust surface structure, thereby improving cycling performance.[6,7] In addition, Mg/Mn co-doping enhances the structural stability of $LiNiO_2$, suppresses nickel dissolution, mitigates electrochemical irreversibility, and improves the cycling stability.[8] Another significant contribution is the comprehensive study by Aurbach and co-workers, who employed a "top-down" approach to

[a] *Materials Science and Engineering, School for Engineering of Matter, Transport and Energy, Arizona State University, Tempe, 85287, USA.*
E-mail: linqinmu@asu.edu
[b] *Stanford Synchrotron Radiation Lightsource, SLAC National Accelerator Laboratory, Menlo Park, CA 94025, USA*
[c] *Center for Functional Nanomaterials, Brookhaven National Laboratory, Upton, New York 11973, USA*

investigate NCM811 doped with various cations, including Mg^{2+}, Al^{3+}, Si^{4+}, Ti^{4+}, Zr^{4+}, and Ta^{5+}.[9] Among these, Ta^{5+} was identified as a particularly promising dopant for enhancing the performance of Ni-rich cathodes. Surface coating is a critical strategy for enhancing the interfacial stability of Ni-rich layered oxide cathodes, as it effectively mitigates surface degradation, transition metal dissolution, and oxygen release under high-voltage cycling conditions.[5] The protective layers have been cataloged into several types: the chemically and electrochemically inactive coatings,[10–12] the Li^+ conductive coatings, mainly referring to the Li-containing compounds,[13–15] and the electron conducting coating.[16–18] These coatings serve as physical and chemical barriers that significantly improve structural integrity and long-term electrochemical performance.

Other than the doping and coating methods, electrolyte formulation plays a crucial role in determining the performance of batteries, influencing their electrochemical properties, electrode stability, and long-term durability, especially under elevated temperatures or cut-off voltages.[19] For instance, we developed localized high-concentration electrolytes (LHCEs) that can enable the formation of effective interfacial layers.[20] Another widely adopted strategy is the incorporation of high-voltage-resistant solvents, including fluorinated carbonates, sulfone-based solvents, and phosphate esters, which enhance oxidative stability and suppress oxygen release from Ni-rich surfaces.[21–23] Additionally, the inclusion of weakly solvating solvents combined with fluorinated lithium salts further refines interfacial compatibility by reducing parasitic reactions and facilitating the construction of a uniform and stable CEI.[24,25] Together, these electrolyte design strategies have been shown to dramatically improve the long-term cycling performance, rate capability, and high-voltage stability of NMC811-based lithium-ion batteries.

In addition, additives are essential components of advanced electrolyte systems, offering diverse chemical functionalities that enhance battery performance.[26,27] A wide range of electrolyte additives have been reported to promote the formation of a thin and stable cathode–electrolyte interphase (CEI), including film-forming agents such as vinylene carbonate (VC),[28] and boron-based additives like tris(trimethylsilyl)borate (TMSB), as well as phosphate/phosphite, fluorinated, sulfur-containing, and silicon-based additives. Amongst these additives, VC has been consistently employed as a standard additive for NMC cathodes, where its oxidation and subsequent polymerization on the particle surface help suppress rock-salt phase formation.[29] In addition, VC serves as an effective lithium stabilizer for lithium metal batteries by promoting the formation of a robust solid electrolyte interphase (SEI) on the Li anode.[28] Additionally, VC can regulate the Li deposition morphology *via* formation of polymeric species on the surface of lithium and improve the uniformity and mechanical strength of the SEI layer.[30,31] Tris(trimethylsilyl)borate (TMSB) was reported to be an efficient film-forming additive on high-voltage cathode materials, to form a thin, dense, and uniform CEI layer consisting of Si–O and B–O bonds.[32] TMSB also prefers to be oxidized compared to the standard electrolyte solution, forming a stable and low-impedance film on the spinel LNCM cathode. Unlike other additives, this doesn't negatively impact the rate capability.[33] In addition, the presence of TMSB in the electrolyte can suppress the electrolyte decomposition and transition metal dissolution.[34,35] In cells with Ni-rich cathodes and lithium metal anodes, degradation of the cathode, *i.e.*, metal dissolution and gas generation, can impact the formation and stability of the solid electrolyte interphase (SEI) on the anode, and *vice versa*. However, existing research primarily focuses on the impact of either the cathode or the anode, leaving a critical gap in understanding how these components interact. In particular, it remains unclear whether the combined use of TMSB and VC as electrolyte additives can effectively enhance the overall stability and performance of Ni-rich Li metal cells. Addressing this gap is crucial for developing a comprehensive strategy to improve battery performance.

In this study, we employed a single-crystal NMC811 cathode and Li metal anodes as the cell platform to systematically revisit the roles of TMSB and VC as electrolyte additives. The cycling performance of cells containing individual (VC or TMSB) and dual VC/TMSB additives in a conventional baseline electrolyte was evaluated at both low and high current rates. Notably, the dual additive system significantly improves long cycling performance, achieving capacity retention of approximately 68%, 67%, and 75.6% after 500 cycles at 1C, 2C, and 5C, respectively, compared to less than 30% retention in cells with the baseline electrolyte alone. Comprehensive electrochemical and spectroscopic analyses revealed that the baseline electrolyte tends to promote LiF accumulation. While single additives (VC or TMSB) initially reduce LiF formation, their effectiveness diminishes with extended cycling, leading to a slight increase in LiF content. In contrast, the dual-additive system maintains a relatively stable, thin CEI, effectively suppressing $LiPF_6$ decomposition and LiF buildup, and leading to a smooth Li deposition after extended cycling. These findings demonstrate the synergistic effect of VC and TMSB in stabilizing the CEI and SEI, thereby improving the performance and longevity of Li-metal batteries. By exploring the dual-additive approach and its impact on both electrodes, this work highlights a promising pathway toward high-efficiency, high-stability lithium metal battery systems.

Results and discussion

We first evaluated the cell performance containing single-crystal $LiNi_{0.83}Mn_{0.06}Co_{0.11}O_2$ (SC-NMC, Fig. S1) as the cathode, Li metal as the anode (SC-NMC||Li), and a baseline electrolyte (BL, LP57 : 1 M $LiPF_6$ dissolved in EC : EMC with a 3 : 7 weight ratio) with or without additives of VC or TMSB (Fig. S2). We are aware that the concentration of electrolyte additives significantly affects the formation of the SEI and CEI. Previous studies identified ~2 wt% VC[36,37] or ~1 wt% TMSB[33,34] as optimal for interfacial stability; therefore, we adopted 2 wt% additives in this work for comparison. Closely examining the initial charge voltage profiles (Fig. 1a) reveals that the cells containing the BL or VC additive exhibit a relatively smooth voltage rise at the very

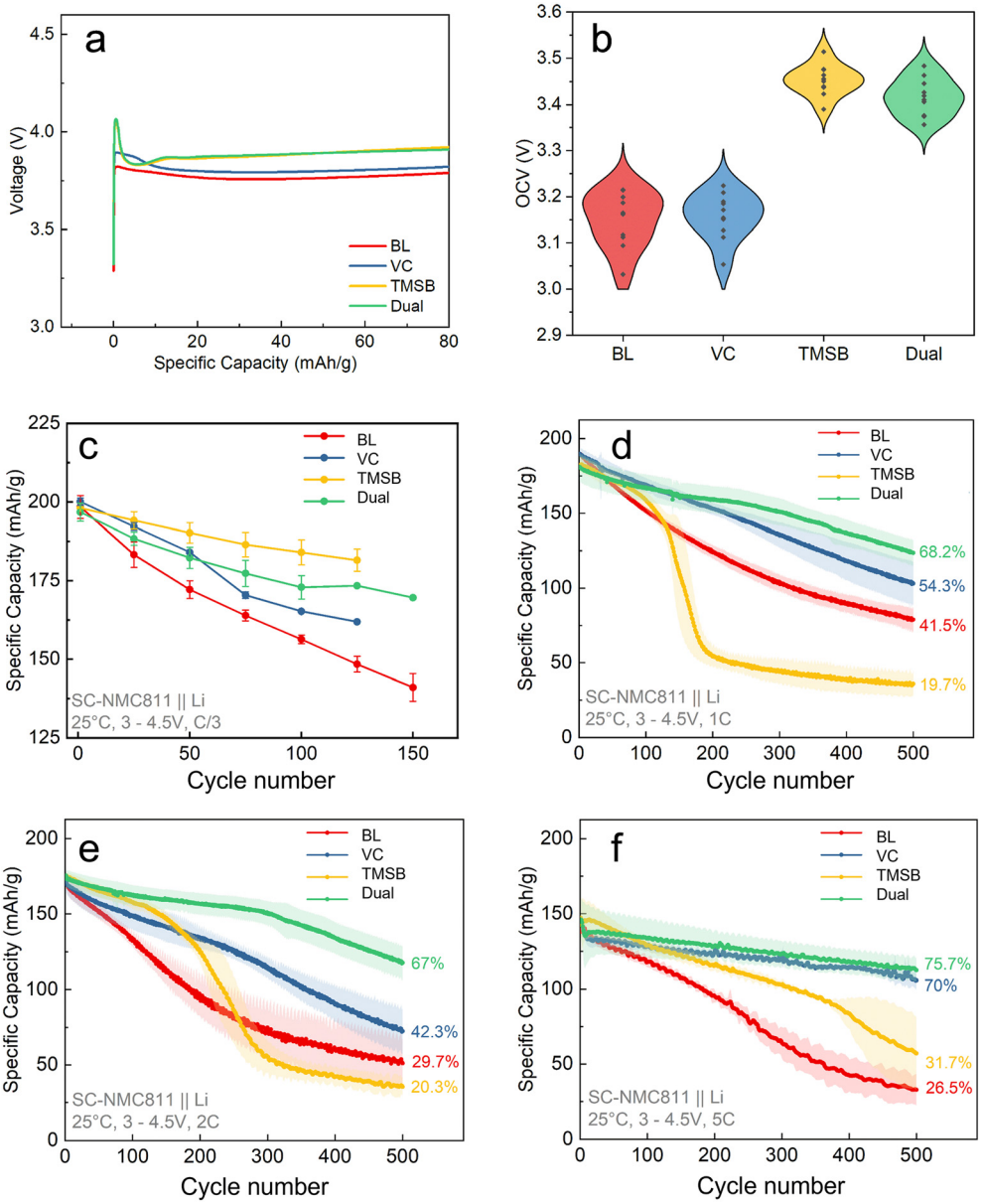

Fig. 1 Battery performance. (a) Initial charge profiles of the cells containing an electrolyte without and with different additives, (b) statistical OCV data as a function of various electrolyte additives, long-term cyclability of cells without and with other additives cycled at C/3 (c), 1C (d), 2C (e), and 5C (f). The cycling data were averaged across at least three cells, and the standard deviations were included to indicate variability. 1C means charge/discharge cells within one hour to 220 mAh g^{-1} capacity. All the cells were cycled within a voltage range of 3.0–4.5 V *vs.* Li/Li^+. BL : 1 M $LiPF_6$ dissolved in EC : EMC with the 3 : 7 weight ratio, VC : BL electrolyte with 2% volume ratio of VC, TMSB : BL electrolyte with 2% volume ratio of TMSB, and dual : BL electrolyte with 2% volume ratio of VC and 2% volume ratio of TMSB.

beginning. In contrast, the cells containing TMSB or dual additives display a pronounced voltage increase, characterized by a distinct voltage hump. In addition, we monitored the open circuit voltage (OCV) of the cells during the resting period before electrochemical cycling (Fig. 1b). For most lithium-ion batteries, the OCV typically ranges from 3.0–3.2 V *vs.* Li/Li^+, reflecting the intrinsic chemical potential difference between the cathode and Li anode, as observed in the cells containing the BL or VC additive. In contrast, the cells containing TMSB-only or dual additives exhibited a relatively higher OCV within 3.3–3.5 V *vs.* Li/Li^+. TMSB can interact with PF_6^- and exert shielding effects on Li^+–anion pairs, thereby altering dipole orientation and the surface electric double-layer. Thus, the slightly elevated OCV may be attributed to the increased electric double-layer potential.[38] In the subsequent electrochemical charging, TMSB begins to decompose and form an interfacial layer, disrupting the initial solvation structure. This interphase formation, coupled with solvation rearrangement, increases cell impedance, consistent with the EIS results, which show a sharp increase in resistance after the activation cycles (Fig. 2f). Consequently, the elevated energy barrier associated with Li^+ extraction manifests as the initial voltage hump.

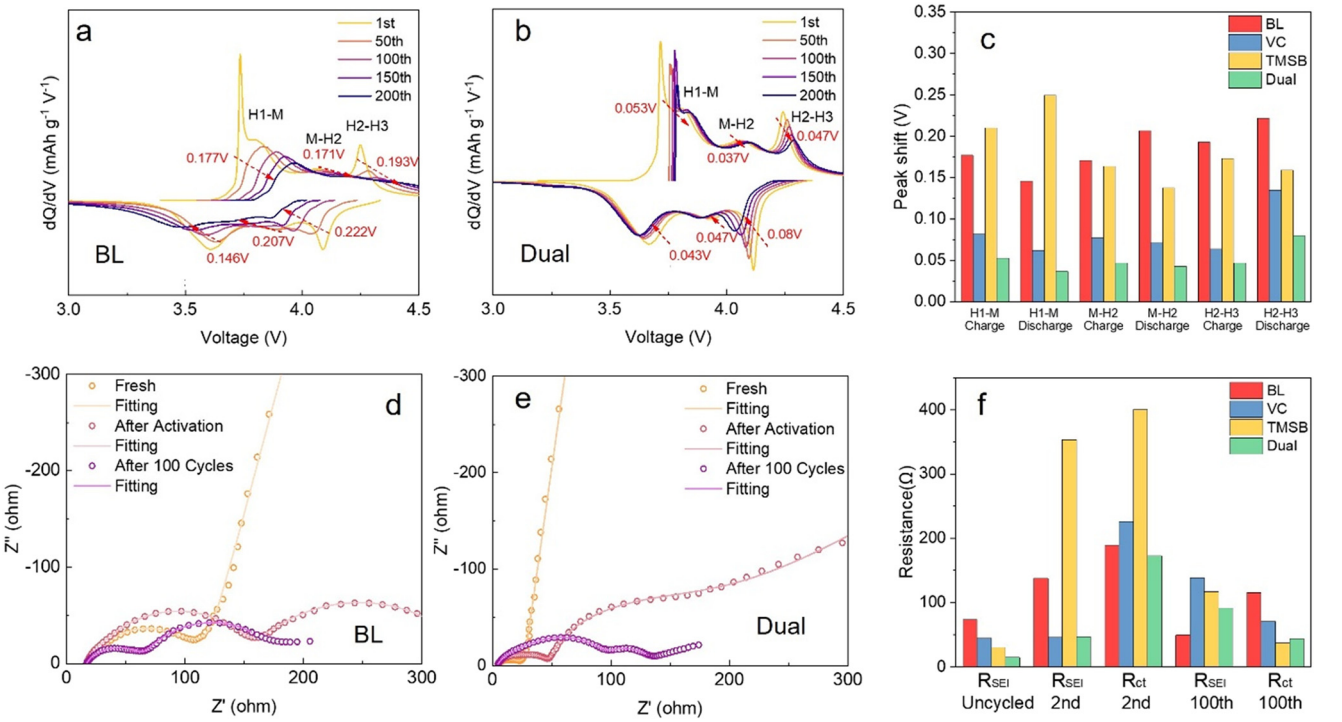

Fig. 2 d*Q*/d*V* and EIS analyses. d*Q*/d*V* curves of the SC-NMC||Li cells cycled at 1C within the voltage range of 3.0–4.5 V *vs.* Li/Li$^+$ in the 1st, 50th, 100th, 150th, and 200th cycles with (a) BL and (b) dual additives. (c) Summary of d*Q*/d*V* peak shifts in SC-NMC||Li cells containing different electrolyte additives after 200 cycles at 1C within the voltage range of 3.0–4.5 V *vs.* Li/Li$^+$. (f) Nyquist plot of the SC-NMC||Li cells before cycling, in the discharge of 3.0 V after two activated cycles at C/3, and after 100 cycles at 2C containing different electrolyte additives: (d) BL and (e) dual additives. (f) Summary of EIS fitting results of the SC-NMC||Li cells containing different electrolyte additives.

To investigate the impact of electrolyte additives under different operating conditions, we assessed the cyclability of cells with and without additives across a range of C-rates (Fig. 1 and S3 and S4), assuming that the applied C-rate affects the formation and distribution of decomposition products at both the cathode and anode interfaces.[39] These interfacial variations can significantly impact the properties of the SEI/CEI, ultimately impacting long-term cycling stability. At C/3, the average initial capacity of 198.4 (BL), 200.1 (VC), 198.1 (TMSB), and 196.8 (dual) mAh g^{-1} was achieved, and the capacity retention was 78.8%, 82.6%, 92.9%, and 87.9%, respectively, after 100 cycles. It was demonstrated that the cells with additives improved the cycling stability, particularly those with the TMSB-only additive. However, the roles of different additives on long-term cycling stability diverge at high C-rates. At 1C, the initial discharge capacities were 189.9, 189.8, 182.3, and 181.1 mAh g^{-1} for cells with BL, VC, TMSB, and dual additives, respectively. After 500 cycles at 1C, the capacity retention varied significantly among the cells with different additives with the retention of 41.5% (BL), 68.2% (VC), 60.3% (TMSB), and 75.0% (dual), respectively. At an even higher current rate, the cells can deliver a capacity retention of 29.7% (BL), 42.3% (VC), 20.3% (TMSB), and 67% (dual) at 2C, and 26.5% (BL), 70% (VC), 31.7% (TMSB), and 75.7% (dual) at 5C after 500 cycles, respectively. Cells with the TMSB-only additive typically exhibit poorer capacity retention at high C-rates (1C, 2C, or 5C) than those cycled at C/3. In contrast, the cells containing dual additives show significantly improved cycling stability. In addition, the coulombic efficiency (CE) of the cells containing the dual additives outperforms those containing the BL or single VC or TMSB additive (Fig. S3). Overall, while TMSB alone enhances cycling stability at the low C-rate but remarkably compromises it at high C-rates, the combination of VC and TMSB offers superior stability under high-rate conditions. The phenomenon further supports that the chemical composition and properties of the EEI layer vary with current density, leading to different cyclability at low and high C-rates. These rate-dependent variations in the composition of the EEI layer are consistent with other reported studies.[39] Additionally, we evaluated the cell performance using a polycrystalline NMC cathode (PC-NMC) and Li metal cycled at both 2C and 5C. The results (Fig. S5) show that cells with dual additives achieve 86.1% (2C) and 85.4% (5C) capacity retention after 300 and 500 cycles, respectively. The capacity retention is significantly higher than that of the cells cycled in BL or with the TMSB additive. The conclusion is consistent with these cells using a SC-NMC cathode. This validates the conclusion that the combined use of VC and TMSB additives exhibits a synergistic effect in stabilizing interfacial formation.

We conducted lithium stripping and plating experiments in Li||Li symmetric cells at 1 mA cm^{-2}, approximating the current density of 1C cycling in the SC-NMC||Li cells (Fig.

S7). The symmetric cells with the BL electrolyte exhibit a relatively stable and flat overpotential around 0.1 V (Fig. S7a). In contrast, those containing electrolytes with additives show noticeable fluctuations in overpotential over 200 hours (Fig. S7b–d). In particular, cells containing the TMSB additive have a much lower initial overpotential, while those with dual additives exhibit a slightly higher initial overpotential. Despite this, all cells maintained stable operation for 200 hours. In contrast, these additives did not effectively enhance the cyclability of symmetric Li cells. As cycling progressed to 400 h (Fig. S8), the stripping/deposition overpotential gradually increased for all cells. This increase was particularly pronounced for cells containing only TMSB, where the overpotential exceeded 0.4 V, whereas cells with the VC/TMSB dual additive maintained overpotentials below 0.3 V. These observations indicate that the dual-additive formulation better stabilizes Li plating/stripping and preserves interfacial integrity on the SC-NMC cathode, while TMSB alone is less effective at suppressing interfacial degradation under extended cycling.

To further investigate the mechanisms behind the performance enhancement observed at high C-rates with the dual additives, we analyzed the evolution of dQ/dV curves and electrochemical impedance of the SC-NMC||Li cells containing different electrolyte formulations at 1C (Fig. 2 and S6). The SC-NMC cathode exhibits three primary redox couples in the dQ/dV curve, corresponding to the phase transformations from H1 to M, M to H2, and H2 to H3 as the voltage increases.[40,41] Typically, the redox couples' peak shifts and intensity reductions indicate structural degradation in the NMC cathode.[42,43] For example, in the cells containing the BL electrolyte (Fig. 2a), the three redox couples consistently shift by approximately 0.17–0.19 V to higher voltages during oxidation and by about 0.15–0.20 V to lower voltages during reduction from the first cycle to 200 cycles. Cells with TMSB showed very similar behavior to those with baseline electrolytes, with shifts of 0.16–0.21 V and 0.14–0.25 V during oxidation and reduction, respectively (Fig. S6a). In contrast, cells containing the VC additive only shifted voltage by 0.06–0.08 V and 0.06–0.13 V during oxidation and reduction, respectively (Fig. S6b). Surprisingly, the cells with the dual additives had the smallest voltage shift, by 0.04–0.05 V and 0.04–0.08 V during oxidation and reduction, respectively (Fig. 2b). In summary, the cells containing the dual additives displayed minimum voltage shifts after 200 cycles, which might be attributed to enhanced structural stability afforded by the robust EEI layer formed on the SC-NMC surface or Li metal surface.

The structural evolution from the surface to bulk, along with the formation of solid-state interfacial layers on both the cathode and anode, contributes to impedance buildup. Thus, we monitored the impedance evolution of cells containing different electrolyte additives at 2C (Fig. 2d–f and S9). In fresh cells, all Nyquist plots exhibit a semicircle followed by a linear slope, corresponding to charge-transfer resistance and Warburg diffusion, respectively. After one cycle, all cells, with or without additives, exhibit two semicircles, as the left-most and second semicircles at high and mid frequencies representing interfacial and charge-transfer resistance, respectively. To decouple impedance evolution, we fitted these spectra using an equivalent circuit (Fig. S10) to quantify impedance changes, and the results are summarized in Fig. 2f and Table S1. In summary, after the formation cycles, cells with VC-only and dual additives exhibited the lowest interfacial impedance, with the dual-additive cell showing the lowest charge transfer resistance. In contrast, the TMSB-only cell displayed the highest interfacial and charge transfer resistance. After 100 cycles, all cells showed a significant reduction in the overall resistance (sum up between interfacial and charge transfer resistance) (Table S1). This suggests that these cells begin forming a thick interfacial layer and periodically dissolve and re-form during the subsequent cycling. Particularly for the cell containing the TMSB additive, it appears that the TMSB additive promotes the formation of the thickest EEI layer, which is also the least stable and tends to dissolve during cycling. This likely contributes to the poorest capacity retention at high C-rates. In contrast, the cell with dual additives maintains the lowest impedance after 100 cycles, aligning with its superior electrochemical performance. The results suggest that the dual additives promote a more stable interface formation and suppress impedance growth.

To correlate impedance and cycling performance with interfacial chemistry, we first conducted soft X-ray absorption spectroscopy (XAS) to examine the surface chemistry of SC-NMC cathodes after activation and 200 cycles at 2C (Fig. 3a–c). Soft XAS in fluorescence yield (FY) and total electron yield (TEY) modes are used to probe electronic states of samples in the subsurface (~50 nm) and surface (~10 nm) regions, respectively.[44] We focused on the Ni L-edge spectrum due to Ni's dominant role in redox reactions in NMC811 and the chemical instability of Ni^{3+} in organic electrolytes. In its pristine state, the Ni nominal oxidation state is approximately +2.875, as indicated by the peak ratio of L_3 to the right/left (Fig. S11). The slightly lower peak ratio in TEY mode relative to the FY mode suggests a more reduced surface in NMC811, associated with some degree of Li^+/Ni^{2+} cation mixing.[45,46] After 200 cycles at 2C, all samples exhibited very similar peak shapes and intensities in FY mode, indicating a comparable bulk Ni oxidation state (Fig. 3a). In contrast, TEY spectra (Fig. 3b) revealed markedly lower surface oxidation states that varied depending on the electrolyte additives, as evidenced by a reduced L_3 right peak. We further quantified the L_3 right/left peak intensity ratio (Fig. 3c) and compared it to $LiNiO_2(Ni^{3+})$ and NMC111(Ni^{2+}) reference materials. These results indicate that the bulk Ni oxidation state after cycling was around +3, slightly higher than the pristine state, likely due to Li-deficiency, consistent with the observed capacity loss. Notably, for all samples except the one cycled with dual VC/TMSB additives, a difference in the ratio between TEY and FY modes was observed. We attribute this difference to a surface-to-bulk oxidation gradient and the extent of surface reconstruction.[7,8]

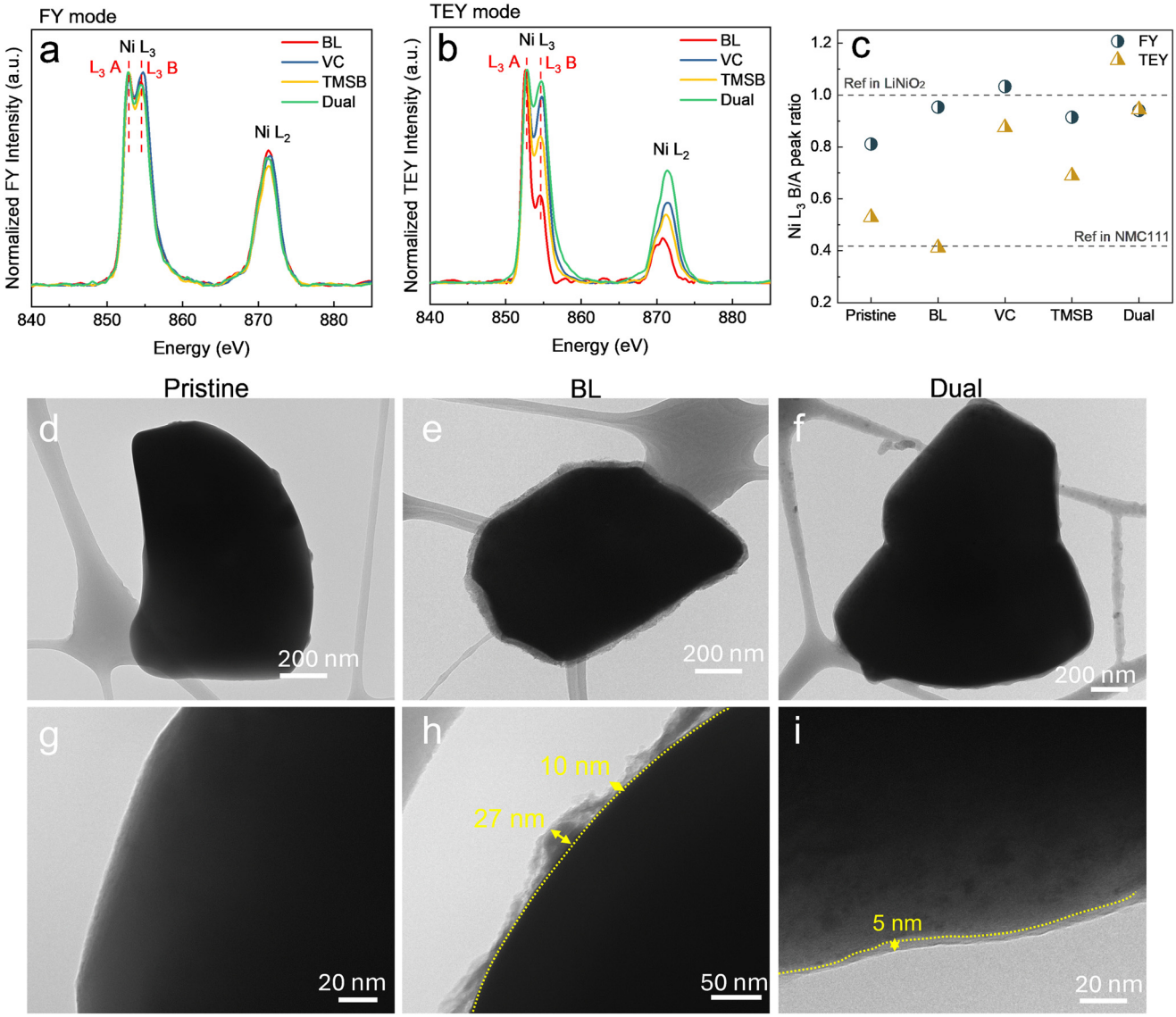

Fig. 3 SC-NMC surface analysis. Nickel L-edge soft XAS in the (a) FY and (b) TEY modes for the SC-NMC cathodes in the discharged state after 200 cycles at 2C within the voltage range of 3.0–4.5 V *vs.* Li/Li^+; (c) the intensity ratio of the L_3 right/left peak is plotted for SC-NMC cycled with different electrolyte additives. Cryo-TEM images of the NMC particles in the pristine state (d and g), cycled at 2C for 100 times in the BL electrolyte (e and h), and cycled at 2C for 100 times with the dual additives (f and i).

SC-NMC cycled in the BL electrolyte exhibited the lowest peak ratio, indicating that the surface Ni was in the lowest oxidation state, consistent with more severe surface degradation and structural changes. Soft XAS analysis demonstrates that the dual-additive electrolyte forms a stable interfacial layer with a more homogeneous chemical and structural distribution from the surface to bulk, effectively protecting the NMC surface.

We performed cryo-TEM analysis on SC-NMC particles in their pristine state and after 200 cycles at 2C, without and with dual additives (Fig. 3d–i). The pristine SC-NMC surface appeared clean and well-defined. However, after electrochemical cycling, the NMC particles became highly fragile under the electron beam, even at very low electron doses, making detailed imaging challenging. Despite this, several particles from each sample were successfully examined. Both cycled NMC samples exhibited a distinct interfacial layer. Although the thickness of the CEI varied among particles, the average CEI thickness on SC-NMC cycled in the baseline electrolyte was approximately 10–30 nm. In contrast, the SC-NMC cycled with dual additives formed a much thinner CEI, typically 3–6 nm. These observations are consistent with the results obtained from soft XAS analysis.

To investigate the chemical composition of the CEI, X-ray Photoelectron Spectroscopy (XPS) was performed on cycled cathode chips, probing C 1s, O 1s, F 1s, B 1s, and Si 2p signals (Fig. 4 and S12 and S13). Each spectrum was deconvoluted into several distinct chemical species or bonding environments through peak fitting (Table S2). After the initial activation cycles, the cathode cycled in the BL electrolyte exhibited the highest levels of carbides, C–O bonds, and LiF, but the lowest C–C,

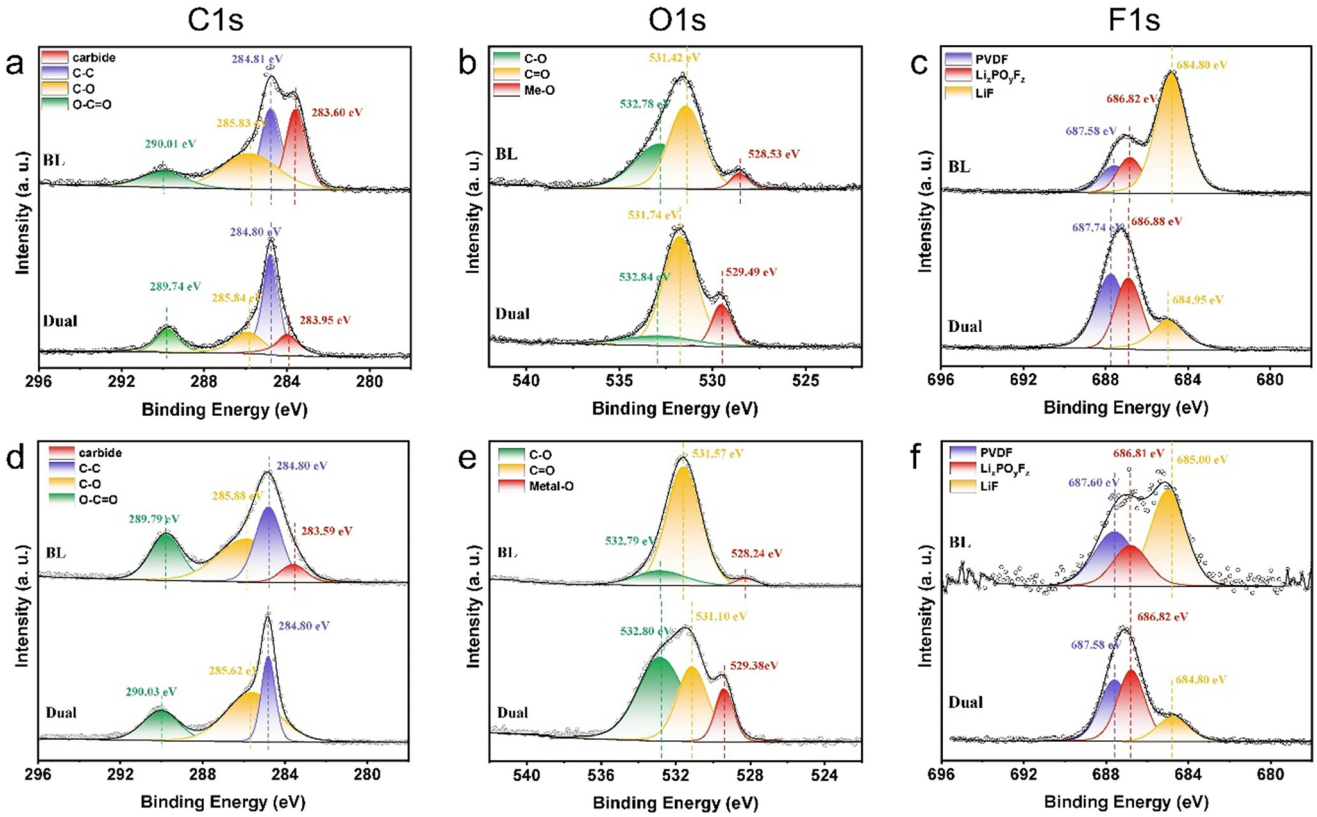

Fig. 4 XPS analysis of the cycled SC-NMC cathodes: (a) C 1s, (b) O 1s and (c) F 1s after the activation cycles and (d) C 1s, (e) O 1s and (f) F 1s after 100 cycles at 2C between 3.0 and 4.5 V.

PVDF, and polymeric $Li_xPO_yF_z$. The carbide (C–Li or C–TM) species may originate from the decomposition of the carbonate solvent, leading to bonding with surface lithium or transition metals that have dissolved from the NMC lattice.[47] This indicates the formation of an initial interfacial layer enriched in inorganic species and deficient in organic components. In contrast, the dual additive electrolyte yielded the highest signal of Me–O (Me = transition metals), PVDF and polymeric species, along with the lowest LiF content, consistent with a thinner CEI that allows detection of bulk Me–O signals and binder-related species embedded in the cathode. Although LiF is often regarded as a stabilizing component,[48–50] our results (in agreement with Hu *et al.*[51,52]) suggest that higher LiF content does not necessarily correlate with improved cycling stability. After 100 cycles, the dual additive sample showed a slight decrease in organic species (C–C and C═O) and an increase in inorganic components (CO_2 and C–O), while Me–O, PVDF, $Li_xPO_yF_z$, and LiF contents remained largely unchanged, indicating minimal CEI thickness evolution. B 1s and Si 2p signals were only detected in cathodes cycled with TMSB-containing electrolytes (sole TMSB and dual additives) after 100 cycles (Fig. S13), suggesting gradual TMSB decomposition into B–O, Si–O, and Si–C species. The presence of Si–C bonds aligns with carbide features in the C 1s spectra, and the absence of these bonds in the dual-additive sample implies that VC suppresses Si–C formation, which may otherwise compromise CEI stability. Overall, the dual-additive electrolyte promotes a robust, LiF-deficient, inorganic-rich CEI with minimal growth over cycling —consistent with the observed impedance trends and electrochemical performance. These findings indicate that achieving long-cycle performance in NMC||Li cells require combined electrolyte additives that foster the formation of a thin, stable, and compositionally optimized CEI layer.

To elucidate the effect of the dual-additive electrolyte on interfacial stability, the Li metal anodes were examined after cycling at 2C (Fig. 5). SEM images clearly distinguish the surface morphologies obtained from different electrolytes (Fig. 5a–c). The Li anode cycled in the BL electrolyte exhibited a porous, mossy, and uneven surface, indicative of uncontrolled Li nucleation and dendritic growth during repeated stripping/plating (Fig. 5b). Such morphology typically leads to increased surface area and continuous electrolyte decomposition. In contrast, the Li anode cycled in the dual-additive electrolyte displayed a compact and uniform surface (Fig. 5c), suggesting that the additives effectively modulate Li^+ flux and promote homogeneous deposition. This morphological improvement implies a stabilized SEI and enhanced cycling durability under high current operation.

To further investigate the interfacial chemistry, XPS analyses of the Li anodes were performed after 100 cycles at 2 C (Fig. 5d–g). The C 1s spectra of both samples reveal similar major SEI components, C–C/C–H, C–O, and O–C═O, suggesting comparable solvent decomposition pathways. A minor O═C–O peak appears in the dual-additive system,

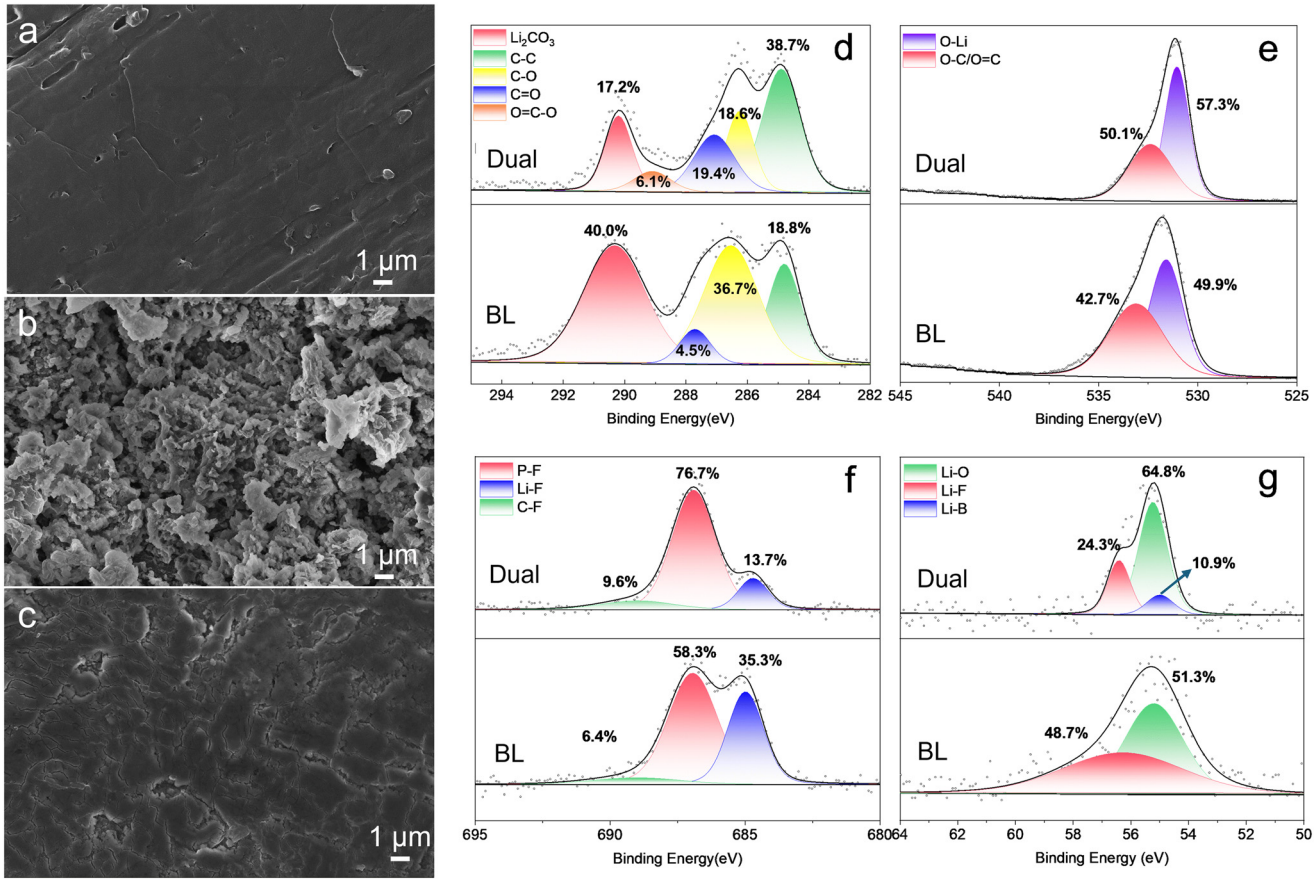

Fig. 5 Li metal anode post analysis. SEM images of the Li metal (a) in the pristine state, after 100 cycles at 2C (b) in the BL electrolyte or (c) with the dual additives; (c) XPS analysis of the Li metal after 100 cycles at 2C of (d) C 1s, (e) O 1s, (f) F 1s, and (g) Li 1s.

likely originating from additional organic carbonate species, indicating slightly increased solvent participation in SEI formation. In addition, Li_2CO_3 is present in lower amounts in the dual additive system. The O 1s spectra show a similar distribution of organic (C═O, C–O) and inorganic (Li_2O, Li_2CO_3) species in both systems, suggesting that the overall organic/inorganic composition of the SEI remains relatively unchanged by the additives. More distinct differences are observed in the F 1s region. Both samples contain P–F and C–F signals, typically derived from $LiPF_6$ decomposition; however, the LiF peak (~685 eV) is notably weaker in the dual-additive electrolyte. The Li 1s spectra corroborate this observation, confirming a reduced LiF content on the anode surface. These results demonstrate that the dual additives suppress $LiPF_6$ decomposition, thereby limiting secondary LiF accumulation on both NMC and Li metal surfaces. Since LiF is an electronically insulating phase that can impede Li^+ transport when overly thick, its suppression leads to a more ionically conductive SEI layer. Collectively, these findings indicate that while the fundamental SEI chemistry remains similar, the dual-additive electrolyte alters the formation kinetics of interfacial species. The resulting SEI possesses lower LiF content and improved uniformity, which effectively reduces interfacial resistance, enhances ion transport, and stabilizes Li deposition during high-rate cycling. This mechanistic understanding of both the cathode and anode explains the superior electrochemical performance and long-term stability of NMC||Li cells employing the dual-additive electrolyte.

Conclusions

In this study, we systematically revisited the role of TMSB and VC electrolyte additives in SC-NMC||Li metal cells, evaluating their individual and combined effects on cycling performance under various current rates. Our results demonstrate that while TMSB increases the OCV and initial overpotential due to the modification in the Li^+ solvation structure and electric double layer, an electrolyte containing the TMSB additive can significantly enhance cyclability at C/3. In particular, the dual-additive system (VC/TMSB) significantly enhances long-term cycling stability at high C-rates, achieving capacity retentions of approximately 68%, 67%, and 75.6% after 500 cycles at 1C, 2C, and 5C, respectively—substantially outperforming the cells in the baseline electrolyte, which retains less than 30% of its initial capacity. Electrochemical and spectroscopic analyses reveal that the BL electrolyte promotes excessive LiF accumulation on both the cathode and anode surfaces. In contrast, the dual-additive formulation synergistically promotes the formation of a thinner, more stable, and LiF-deficient EEI. This robust EEI effectively

suppresses surface structural degradation of the NMC cathode and mitigates overall cell impedance growth during extended cycling. Overall, this work elucidates the synergistic function of VC and TMSB at both electrodes, offering valuable insights into co-additive design for advancing high-energy lithium metal battery technology.

Author contributions

L. M. led the project and designed the experiments. Z. Z. and Y. L. performed electrochemical cycling, XRD, and XPS experiments. Y. Z. assisted XPS and XAS data collection and analysis. D. Nordlund performed soft XAS measurements. S. H. performed the cryo-TEM images. L. M. wrote the manuscript with the help of all the co-authors.

Conflicts of interest

There are no conflicts to declare.

Data availability

Data for this article, including raw data and processed data for figures in the main text and supplementary information (SI) are available at Zenodo at https://zenodo.org/records/18485537.

The data supporting this article have been included as part of the SI.

Supplementary information: experimental details (electrode preparation, cell testing, symmetric cells, characterization details), supporting figures and supporting tables. See DOI: https://doi.org/10.1039/d5lf00236b.

Acknowledgements

This work was supported by the start-up funding provided by the Materials Science and Engineering, School for Engineering of Matter, Transport and Energy at Arizona State University. The authors acknowledge the use of XPS, XRD, and SEM facilities within the Eyring Materials Center at Arizona State University, supported in part by NNCI-ECCS-2025490. The authors also thank Xin Guo at the Eyring Materials Center for scientific discussion on XPS results. The use of soft XAS at the Stanford Synchrotron Radiation Lightsource (SSRL) at the SLAC National Accelerator Laboratory is supported by the U.S. Department of Energy, Office of Science, Office of Basic Energy Sciences under Contract No. DE-AC02-76SF00515. This research used the electron microscopy facility of the Center for Functional Nanomaterials (CFN), which is a U.S. Department of Energy Office of Science User Facility, at Brookhaven National Laboratory under Contract No. DE-SC0012704.

References

1 S.-T. Myung, F. Maglia, K.-J. Park, C. S. Yoon, P. Lamp, S.-J. Kim and Y.-K. Sun, Nickel-Rich Layered Cathode Materials for Automotive Lithium-Ion Batteries: Achievements and Perspectives, *ACS Energy Lett.*, 2017, **2**(1), 196–223.

2 J.-M. Kim, X. Zhang, J.-G. Zhang, A. Manthiram, Y. S. Meng and W. Xu, A review on the stability and surface modification of layered transition-metal oxide cathodes, *Mater. Today*, 2021, **46**, 155–182.

3 J. Kim, H. Lee, H. Cha, M. Yoon, M. Park and J. Cho, Prospect and Reality of Ni-Rich Cathode for Commercialization, *Adv. Energy Mater.*, 2018, **8**(6), 1702028.

4 J. Xiao, N. Adelstein, Y. Bi, W. Bian, J. Cabana, C. L. Cobb, Y. Cui, S. J. Dillon, M. M. Doeff, S. M. Islam, K. Leung, M. Li, F. Lin, J. Liu, H. Luo, A. C. Marschilok, Y. S. Meng, Y. Qi, R. Sahore, K. G. Sprenger, R. C. Tenent, M. F. Toney, W. Tong, L. F. Wan, C. Wang, S. E. Weitzner, B. Wu and Y. Xu, Assessing cathode–electrolyte interphases in batteries, *Nat. Energy*, 2024, **9**(12), 1463–1473.

5 L. Liang, W. Zhang, F. Zhao, D. K. Denis, F. u. Zaman, L. Hou and C. Yuan, Surface/Interface Structure Degradation of Ni-Rich Layered Oxide Cathodes toward Lithium-Ion Batteries: Fundamental Mechanisms and Remedying Strategies, *Adv. Mater. Interfaces*, 2020, **7**(3), 1901749.

6 L. Mu, R. Zhang, W. H. Kan, Y. Zhang, L. Li, C. Kuai, B. Zydlewski, M. M. Rahman, C.-J. Sun, S. Sainio, M. Avdeev, D. Nordlund, H. L. Xin and F. Lin, Dopant Distribution in Co-Free High-Energy Layered Cathode Materials, *Chem. Mater.*, 2019, **31**(23), 9769–9776.

7 L. Mu, Z. Yang, L. Tao, C. K. Waters, Z. Xu, L. Li, S. Sainio, Y. Du, H. L. Xin, D. Nordlund and F. Lin, The sensitive surface chemistry of Co-free, Ni-rich layered oxides: identifying experimental conditions that influence characterization results, *J. Mater. Chem. A*, 2020, **8**(34), 17487–17497.

8 L. Mu, W. H. Kan, C. Kuai, Z. Yang, L. Li, C.-J. Sun, S. Sainio, M. Avdeev, D. Nordlund and F. Lin, Structural and Electrochemical Impacts of Mg/Mn Dual Dopants on the LiNiO2 Cathode in Li-Metal Batteries, *ACS Appl. Mater. Interfaces*, 2020, **12**(11), 12874–12882.

9 T. Weigel, F. Schipper, E. M. Erickson, F. A. Susai, B. Markovsky and D. Aurbach, Structural and Electrochemical Aspects of LiNi0.8Co0.1Mn0.1O2 Cathode Materials Doped by Various Cations, *ACS Energy Lett.*, 2019, **4**(2), 508–516.

10 S.-G. Woo, J.-H. Han, K. J. Kim, J.-H. Kim, J.-S. Yu and Y.-J. Kim, Surface modification by sulfated zirconia on high-capacity nickel-based cathode materials for Li-ion batteries, *Electrochim. Acta*, 2015, **153**, 115–121.

11 W. Liu, X. Li, D. Xiong, Y. Hao, J. Li, H. Kou, B. Yan, D. Li, S. Lu, A. Koo, K. Adair and X. Sun, Significantly improving cycling performance of cathodes in lithium ion batteries: The effect of Al2O3 and LiAlO2 coatings on LiNi0.6Co0.2Mn0.2O2, *Nano Energy*, 2018, **44**, 111–120.

12 Y. Wu, H. Ming, M. Li, J. Zhang, W. Wahyudi, L. Xie, X. He, J. Wang, Y. Wu and J. Ming, New Organic Complex for Lithium Layered Oxide Modification: Ultrathin Coating, High-Voltage, and Safety Performances, *ACS Energy Lett.*, 2019, **4**(3), 656–665.

13 L. Li, Z. Chen, Q. Zhang, M. Xu, X. Zhou, H. Zhu and K. Zhang, A hydrolysis-hydrothermal route for the synthesis of ultrathin LiAlO2-inlaid LiNi0.5Co0.2Mn0.3O2 as a high-

performance cathode material for lithium ion batteries, *J. Mater. Chem. A*, 2015, **3**(2), 894–904.

14 D. Wang, X. Li, Z. Wang, H. Guo, Z. Huang, L. Kong and J. Ru, Improved high voltage electrochemical performance of Li2ZrO3-coated LiNi0.5Co0.2Mn0.3O2 cathode material, *J. Alloys Compd.*, 2015, **647**, 612–619.

15 J. Xie, A. D. Sendek, E. D. Cubuk, X. Zhang, Z. Lu, Y. Gong, T. Wu, F. Shi, W. Liu, E. J. Reed and Y. Cui, Atomic Layer Deposition of Stable LiAlF4 Lithium Ion Conductive Interfacial Layer for Stable Cathode Cycling, *ACS Nano*, 2017, **11**(7), 7019–7027.

16 L. Liang, C. Wu, X. Sun, X. Sun, L. Hou, J. Sun and C. Yuan, Sur-/Interface Engineering of Hierarchical LiNi0.6Mn0.2Co0.2O2@LiCoPO4@Graphene Architectures as Promising High-Voltage Cathodes toward Advanced Li-Ion Batteries, *Adv. Mater. Interfaces*, 2017, **4**(14), 1700382.

17 Y.-S. Lee, W.-K. Shin, A. G. Kannan, S. M. Koo and D.-W. Kim, Improvement of the Cycling Performance and Thermal Stability of Lithium-Ion Cells by Double-Layer Coating of Cathode Materials with Al2O3 Nanoparticles and Conductive Polymer, *ACS Appl. Mater. Interfaces*, 2015, **7**(25), 13944–13951.

18 Q. Gan, N. Qin, Y. Zhu, Z. Huang, F. Zhang, S. Gu, J. Xie, K. Zhang, L. Lu and Z. Lu, Polyvinylpyrrolidone-Induced Uniform Surface-Conductive Polymer Coating Endows Ni-Rich LiNi0.8Co0.1Mn0.1O2 with Enhanced Cyclability for Lithium-Ion Batteries, *ACS Appl. Mater. Interfaces*, 2019, **11**(13), 12594–12604.

19 Y.-K. Liu, C.-Z. Zhao, J. Du, X.-Q. Zhang, A.-B. Chen and Q. Zhang, Research Progresses of Liquid Electrolytes in Lithium-Ion Batteries, *Small*, 2023, **19**(8), 2205315.

20 X. Zhang, H. Jia, L. Zou, Y. Xu, L. Mu, Z. Yang, M. H. Engelhard, J.-M. Kim, J. Hu, B. E. Matthews, C. Niu, C. Wang, H. Xin, F. Lin and W. Xu, Electrolyte Regulating toward Stabilization of Cobalt-Free Ultrahigh-Nickel Layered Oxide Cathode in Lithium-Ion Batteries, *ACS Energy Lett.*, 2021, **6**(4), 1324–1332.

21 D. Ouyang, K. Wang, Y. Pang and Z. Wang, A fluorinated carbonate-based electrolyte for high-voltage Li(Ni0.8Mn0.1Co0.1)O2 lithium-ion cells, *J. Power Sources*, 2022, **529**, 231247.

22 Q. Zhao, Y. Wu, Z. Yang, D. Song, X. Sun, C. Wang, L. Yang, Y. Zhang, J. Gao, T. Ohsaka, F. Matsumoto and J. Wu, A fluorinated electrolyte stabilizing high-voltage graphite/NCM811 batteries with an inorganic-rich electrode-electrolyte interface, *Chem. Eng. J.*, 2022, **440**, 135939.

23 J. Holoubek, M. Yu, S. Yu, M. Li, Z. Wu, D. Xia, P. Bhaladhare, M. S. Gonzalez, T. A. Pascal, P. Liu and Z. Chen, An All-Fluorinated Ester Electrolyte for Stable High-Voltage Li Metal Batteries Capable of Ultra-Low-Temperature Operation, *ACS Energy Lett.*, 2020, **5**(5), 1438–1447.

24 Y. Guo, M. Miao, Y.-X. Wang, C. Yan, J. Liu, Y. Cao, H. Yang, X. Ai and F.-S. Ke, A high-voltage and low-solvating electrolyte towards promising micro-Si/Ni-rich NMC full cells, *Energy Storage Mater.*, 2024, **67**, 103258.

25 J. Guo, F. Hai, W. Chen, X. Gao, Y. Yi, W. Xue, W. Tang and M. Li, Weak Solvation Chemistry in Fluorinated Nonflammable Electrolytes Achieves Stable Cycling in High-Voltage Lithium Metal Batteries, *ACS Appl. Mater. Interfaces*, 2024, **16**(24), 31056–31066.

26 A. M. Haregewoin, A. S. Wotango and B.-J. Hwang, Electrolyte additives for lithium ion battery electrodes: progress and perspectives, *Energy Environ. Sci.*, 2016, **9**(6), 1955–1988.

27 H. Zhang, G. G. Eshetu, X. Judez, C. Li, L. M. Rodriguez-Martínez and M. Armand, Electrolyte Additives for Lithium Metal Anodes and Rechargeable Lithium Metal Batteries: Progress and Perspectives, *Angew. Chem., Int. Ed.*, 2018, **57**(46), 15002–15027.

28 Y. Qian, C. Schultz, P. Niehoff, T. Schwieters, S. Nowak, F. M. Schappacher and M. Winter, Investigations on the electrochemical decomposition of the electrolyte additive vinylene carbonate in Li metal half cells and lithium ion full cells, *J. Power Sources*, 2016, **332**, 60–71.

29 H. Dai, L. Gomes, D. Maxwell, S. Zamani, K. Yang, D. Atienza, N. Dale and S. Mukerjee, Exploring the Role of an Electrolyte Additive in Suppressing Surface Reconstruction of a Ni-Rich NMC Cathode at Ultrahigh Voltage via Enhanced In Situ and Operando Characterization Methods, *ACS Appl. Mater. Interfaces*, 2024, **16**(7), 8639–8654.

30 Y. Yang, J. Xiong, S. Lai, R. Zhou, M. Zhao, H. Geng, Y. Zhang, Y. Fang, C. Li and J. Zhao, Vinyl Ethylene Carbonate as an Effective SEI-Forming Additive in Carbonate-Based Electrolyte for Lithium-Metal Anodes, *ACS Appl. Mater. Interfaces*, 2019, **11**(6), 6118–6125.

31 Z. L. Brown, S. Jurng and B. L. Lucht, Investigation of the Lithium Solid Electrolyte Interphase in Vinylene Carbonate Electrolytes Using Cu||LiFePO4 Cells, *J. Electrochem. Soc.*, 2017, **164**(9), A2186.

32 J. Wang, H. Dong, P. Wang, X.-L. Fu, N.-S. Zhang, D.-N. Zhao, S.-Y. Li and X.-L. Cui, Adjusting the solvation structure with tris(trimethylsilyl)borate additive to improve the performance of LNCM half cells, *J. Energy Chem.*, 2022, **67**, 55–64.

33 Z. Wang, L. Xing, J. Li, B. Li, M. Xu, Y. Liao and W. Li, Trimethyl borate as an electrolyte additive for high potential layered cathode with concurrent improvement of rate capability and cyclic stability, *Electrochim. Acta*, 2015, **184**, 40–46.

34 H. Rong, M. Xu, B. Xie, X. Liao, W. Huang, L. Xing and W. Li, Tris (trimethylsilyl) borate (TMSB) as a cathode surface film forming additive for 5V Li/LiNi0.5Mn1.5O4 Li-ion cells, *Electrochim. Acta*, 2014, **147**, 31–39.

35 F. Zou, J. Wang, X. Zheng, X. Hu, J. Wang and M. Wang, Improved interfacial properties of LiNi0.8Co0.15Al0.05O2 cathode by tris(trimethylsilyl) borate as an electrolyte additive to inhibit HF formation, *Electrochim. Acta*, 2022, **428**, 140958.

36 L. Madec, J. Xia, R. Petibon, K. J. Nelson, J.-P. Sun, I. G. Hill and J. R. Dahn, Effect of Sulfate Electrolyte Additives on LiNi1/3Mn1/3Co1/3O2/Graphite Pouch Cell Lifetime: Correlation between XPS Surface Studies and Electrochemical Test Results, *J. Phys. Chem. C*, 2014, **118**(51), 29608–29622.

37 L. Madec, R. Petibon, J. Xia, J. P. Sun, I. G. Hill and J. R. Dahn, Understanding the Role of Prop-1-ene-1,3-Sultone and Vinylene Carbonate in LiNi1/3Mn1/3Co1/3O2/Graphite Pouch Cells: Electrochemical, GC-MS and XPS Analysis, *J. Electrochem. Soc.*, 2015, **162**(14), A2635.

38 Y.-K. Han, K. Lee, J. Yoo and Y. S. Huh, Virtual screening of borate derivatives as high-performance additives in lithium-ion batteries, *Theor. Chem. Acc.*, 2014, **133**(10), 1562.

39 A. Swiderska-Mocek, A. Gabryelczyk, M. Popławski and A. Lewandowski, Unveiling factors affecting the solid electrolyte interphase resistance: the effect of real surface area and particle size of electrode materials, *J. Solid State Electrochem.*, 2025, **29**(11), 4803–4817.

40 S.-M. Bak, E. Hu, Y. Zhou, X. Yu, S. D. Senanayake, S.-J. Cho, K.-B. Kim, K. Y. Chung, X.-Q. Yang and K.-W. Nam, Structural Changes and Thermal Stability of Charged LiNixMnyCozO2 Cathode Materials Studied by Combined In Situ Time-Resolved XRD and Mass Spectroscopy, *ACS Appl. Mater. Interfaces*, 2014, **6**(24), 22594–22601.

41 S. S. Zhang, Problems and their origins of Ni-rich layered oxide cathode materials, *Energy Storage Mater.*, 2020, **24**, 247–254.

42 J. Choi, L. Dong, C.-Y. Yu, C. O'Meara, E. Lee and J.-H. Kim, Relationship of Chemical Composition and Moisture Sensitivity in LiNixMnyCo1−X−YO2 for Lithium-Ion Batteries, *J. Electrochem. Energy Convers. Storage*, 2021, **18**(4), 041009.

43 F. Pfeiffer, D. Diddens, M. Weiling, L. Frankenstein, S. Kühn, I. Cekic-Laskovic and M. Baghernejad, Quadrupled Cycle Life of High-Voltage Nickel-Rich Cathodes: Understanding the Effective Thiophene-Boronic Acid-Based CEI via Operando SHINERS, *Adv. Energy Mater.*, 2023, **13**(25), 2300827.

44 F. Lin, D. Nordlund, I. M. Markus, T.-C. Weng, H. L. Xin and M. M. Doeff, Profiling the nanoscale gradient in stoichiometric layered cathode particles for lithium-ion batteries, *Energy Environ. Sci.*, 2014, **7**(9), 3077–3085.

45 C. D. Quilty, P. J. West, G. P. Wheeler, L. M. Housel, C. J. Kern, K. R. Tallman, L. Ma, S. Ehrlich, C. Jaye, D. A. Fischer, K. J. Takeuchi, D. C. Bock, A. C. Marschilok and E. S. Takeuchi, Elucidating Cathode Degradation Mechanisms in LiNi0.8Mn0.1Co0.1O2 (NMC811)/Graphite Cells Under Fast Charge Rates Using Operando Synchrotron Characterization, *J. Electrochem. Soc.*, 2022, **169**(2), 020545.

46 Y. Lu, T. Zhu, E. McShane, B. D. McCloskey and G. Chen, Single-Crystal LiNixMnyCo1−x−yO2 Cathodes for Extreme Fast Charging, *Small*, 2022, **18**(12), 2105833.

47 J. Langdon and A. Manthiram, Crossover Effects in Batteries with High-Nickel Cathodes and Lithium-Metal Anodes, *Adv. Funct. Mater.*, 2021, **31**(17), 2010267.

48 T. Chen, J. You, R. Li, H. Li, Y. Wang, C. Wu, Y. Sun, L. Yang, Z. Ye, B. Zhong, Z. Wu and X. Guo, Ultra-Low Concentration Electrolyte Enabling LiF-Rich SEI and Dense Plating/Stripping Processes for Lithium Metal Batteries, *Adv. Sci.*, 2022, **9**(28), 2203216.

49 S. Chen, X. Meng, D. Han, S. Chen, J. Zhou, M. Wang, J. Wang, Z. Wang, C. W. Bielawski and J. Geng, A covalently bonded, LiF-rich solid electrolyte interphase for Li metal batteries with superior low-temperature performance, *Chem. Eng. J.*, 2024, **500**, 156909.

50 Y. Liu, X. Tao, Y. Wang, C. Jiang, C. Ma, O. Sheng, G. Lu and X. W. Lou, Self-assembled monolayers direct a LiF-rich interphase toward long-life lithium metal batteries, *Science*, 2022, **375**(6582), 739–745.

51 M. M. Rahman, S. Tan, Y. Yang, H. Zhong, S. Ghose, I. Waluyo, A. Hunt, L. Ma, X.-Q. Yang and E. Hu, An inorganic-rich but LiF-free interphase for fast charging and long cycle life lithium metal batteries, *Nat. Commun.*, 2023, **14**(1), 8414.

52 M. Mominur Rahman and E. Hu, Electron Delocalization Enables Sulfone-based Single-solvent Electrolyte for Lithium Metal Batteries, *Angew. Chem., Int. Ed.*, 2023, **62**(44), e202311051.